



Dissolution of molybdenum current collector as Crucial and Undesired process in aluminum batteries

Eugen Zemlyanushin^{a,**} , Björn Schwarz^a , Sonia Dsoke^{a,b,c,*}

^a Institute for Applied Materials (IAM), Karlsruhe Institute of Technology (KIT), Hermann-von-Helmholtz Platz 1, 76344 Eggenstein-Leopoldshafen, Germany

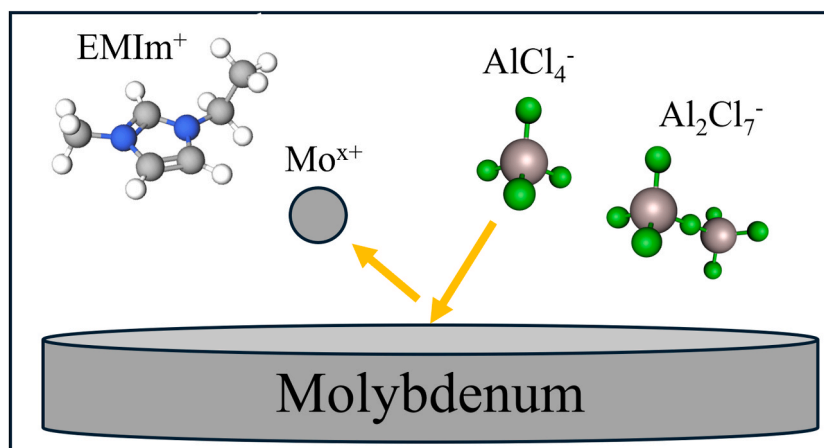
^b Albert-Ludwigs University Freiburg, Department of Sustainable Systems Engineering (INATECH), Emmy-Noether-Straße 2, 79110, Freiburg, Germany

^c Fraunhofer Institute for Solar Energy Systems, Department of Electrical Energy Storage, Heidenhofstr. 2, 79119, Freiburg, Germany

HIGHLIGHTS

- Instability of current collector for rechargeable aluminum batteries revealed.
- Dissolution of molybdenum in acidic AlCl₃:EMImCl (1.5:1) ionic liquid electrolyte.
- Formation of redox-active Mo-complexes.
- Additional capacity due to parasitic side reactions.
- The reactivity of molybdenum is not negligible.

GRAPHICAL ABSTRACT



ARTICLE INFO

Keywords:

Rechargeable aluminum batteries (RABs)
Molybdenum
Ionic liquid electrolyte
Current collector

ABSTRACT

Rechargeable aluminum batteries (RABs) using Lewis acidic aluminum chloride–1-ethyl-3-methylimidazolium chloride (AlCl₃-EMImCl) ionic liquid electrolytes are promising alternative energy storage systems. Molybdenum (Mo), often used as a current collector, is typically considered stable with negligible redox activity in such electrolytes. However, this study shows that Mo reacts with AlCl₃-EMImCl (1.5:1) electrolyte. When Mo-foil or powder is immersed, the initially colorless/yellowish ionic liquid turns red, indicating Mo dissolution. Magnetometry confirms the presence of Mo species with localized unpaired electrons in the red liquid, not found in metallic Mo. UV–VIS spectroscopy reveals Mo³⁺ and Mo⁴⁺ species formation. ICP-OES shows 1.99 ± 0.06 mass-% of Mo dissolves in the electrolyte. Due to Mo's instability, cyclic voltammetry (CV) and galvanostatic cycling with potential limitation (GCPL) show increasing redox activity over cycles, similar to unstable platinum (Pt), with a discharge capacity of ~136 mAh·g⁻¹ at 20 mA·g⁻¹ after 100 cycles. X-ray photoelectron spectroscopy (XPS)

* Corresponding author. Institute for Applied Materials (IAM), Karlsruhe Institute of Technology (KIT), Hermann-von-Helmholtz Platz 1, 76344 Eggenstein-Leopoldshafen, Germany.

** Corresponding author.

E-mail addresses: eugen.zemlyanushin@kit.edu (E. Zemlyanushin), sonia.dsoke@ise.fraunhofer.de (S. Dsoke).

<https://doi.org/10.1016/j.jpowsour.2025.236458>

Received 12 November 2024; Received in revised form 24 January 2025; Accepted 2 February 2025

Available online 13 February 2025

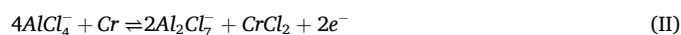
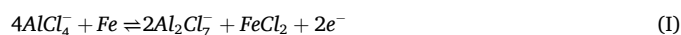
0378-7753/© 2025 The Authors. Published by Elsevier B.V. This is an open access article under the CC BY license (<http://creativecommons.org/licenses/by/4.0/>).

indicates three oxidation states of Mo^{4+/5+/6+} on the aluminum negative electrode, due to Mo-cation migration and adsorption. Covering the Mo current collector with electrochemically inactive Co₃O₄ suppresses Mo reactivity by reducing active Mo surface area. These findings demonstrate Mo's significant impact on AlCl₃-based RABs' electrochemical performance, which is not negligible.

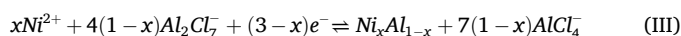
1. Introduction

Nowadays, due to the increased need for electric energy, the focus has shifted to generate energy from renewable sources. For example, mankind already uses wind energy, solar energy, or produces energy via geothermal heat, as well as hydro-energy [1]. However, the challenge is to store this energy and to be able to use it at any time. Thus, high-performance energy storage devices are required. To date, the most advanced rechargeable batteries for wide application are lithium (Li)-nickel (Ni)- manganese (Mn)- cobalt (Co)- oxides (NMC) [2]. Unfortunately, worldwide lithium resources are limited, just like cobalt is often mined under morally reprehensible conditions [3,4]. Therefore, the demand for alternative battery systems has increased and the need for research is indispensable. As a potential successor of lithium and sodium (Na)-based batteries, aluminum (Al) has become one of the most promising candidates [5,6]. The low price and high stability at ambient atmosphere make Al an ideal metal for use in batteries. In theory, Al can provide a specific capacity of 2980 mAh·g⁻¹ which is comparable to Li (3860 mAh·g⁻¹) while the volumetric capacity of 8040 mAh·cm⁻³ is circa four times higher than that of Li with 2060 mAh·cm⁻³ [7–13]. However, Al tends to form a passivation layer of non-conductive aluminum oxide (Al₂O₃) on the surface, which harms the plating and stripping ability [9, 13]. To remove the Al₂O₃ surface layer, it is necessary to use a Lewis acidic ionic liquid electrolyte made of aluminum chloride (AlCl₃) and 1-ethyl-3-methylimidazolium chloride (EMImCl) with a molar ratio >1 for AlCl₃, since otherwise the formation of needed Al₂Cl₇⁻ would be prohibited [14]. Latest findings prove that the ratio of 1.5:1 is the ideal compromise between plating/stripping ability and corrosion effects [14–16]. Furthermore, the ionic liquid forms the AlCl₄⁻ complex which can intercalate into the host lattice of the cathode materials (graphite for instance). Since the high charge density of Al³⁺ results in numerous interactions inside the host lattice of any material that lead to slow kinetics, Al³⁺ cannot be used and must be complexed by chloride anions. On the other hand, because of the high Lewis acidity of such ionic liquid electrolytes, the pure Al negative electrode suffers from pulverization, formation of inactive Al, formation of dendrites, and corrosion [17]. Furthermore, AlCl₃-based ionic liquid (IL) electrolytes are costly, sensitive to air and moisture, and they have a low anodic limit potential making it impossible for positive cathode materials, like metal-oxides (V₂O₅) [18] or -sulfides (Ni₃S₂) [19], to be charged to high voltage, reducing the available energy density. At high potentials, side reactions through the decomposition of the electrolyte and evolution of chlorine (Cl₂)-gas are occurring. The anodic limiting potential of the AlCl₃:EMImCl electrolyte is reported to be less than 2.6 V (vs. Al) and becomes lower with increasing amount of AlCl₃ (1.8 V (vs. Al) at a ratio of 2:1) [13]. The selection of the cut-off voltage for charging is one example of controversial data in the literature because, Jiao et al. [17], for instance, reported a maximum limit of 2.3 V vs. Al for the 1.5:1 ratio electrolyte. It is worth noting that common aluminum chalcogen batteries such as sulfur (S), selenium (Se), and tellurium (Te)-based ones, suffer from capacity loss because of their chemical dissolution and even the dissolution of the oxidation products of the cathode into the electrolyte [13, 20,21]. Furthermore, due to electrochemical decomposition and dissolution, the active materials can detach from the current collector and solubilize into the ionic liquid and migrate/deposit on the negative electrode (shuttle-effect) [2,13]. The same behavior has been observed for the common V₂O₅ cathode compound [22]. It seems that all electrophilic elements (oxygen (O), S, Se, and Te) of the VI A group react and interact with the AlCl₃/EMImCl electrolyte [13,23]. However, in the

early stage of investigations, several reports describe V₂O₅ to be a great cathode material for AlCl₃-based RABs [18,24,25]. In 2011, Jayaprakash et al. [18] reported V₂O₅ to be a suitable Al³⁺ intercalation cathode material. The active material was coated on stainless steel (SS) and the measurements were done in SS coin cells. Two years later, Reed et al. [26] demonstrated that the whole electrochemical contribution came from the SS and not from the V₂O₅. The containing elements of SS, iron (Fe), and chromium (Cr) react with the AlCl₃-based ionic liquid to the corresponding metal chlorides [26] (Eq. I and II):



In 2015, Wang et al. [24] replaced the SS by a nickel (Ni) foam as a current collector and the V₂O₅ positive electrode gave an initial discharge capacity of 239 mAh·g⁻¹. Three years later, the reactivity between Ni and the AlCl₃:EMImCl (1.3:1) ionic liquid electrolyte has been demonstrated by Oh et al. [27] and the suggested reaction is shown below (Eq. III):



The reaction of Ni occurs already while immersion into the ionic liquid electrolyte. Additionally, NiO and Ni₂O₃ formed on the surface by soaking the Ni metal for 10–30 days in the electrolyte as has been proven by XPS [27]. Similar to those results, tungsten (W) is mentioned to react with the electrolyte [27]. Obviously, it is difficult to find a stable current collector material for RABs. Therefore, Wang et al. [28] published an overview of suitable and unsuitable current collector materials in the potential range of 0 to 2.5 V vs. Al while using the strongest Lewis acidic ionic liquid electrolyte with the molar ratio of 2:1 (AlCl₃:EMImCl). The authors describe that Cr, SS, Al, titanium (Ti), and even gold (Au) are not suitable for AlCl₃:EMImCl-based RABs. They report a higher stability for molybdenum (Mo), glassy carbon (GC), tungsten (W), chromium nitride (Cr₂N), and titanium nitride (TiN). Nickel is not mentioned although it has been the most common current collector for RABs until 2018 [29, 30]. While Oh et al. [27] reported Mo to be more stable than W in an even lower Lewis acidic electrolyte with a ratio of 1.3:1, Wang et al. [28] describe the opposite. Further, Chen et al. [31] propose tantalum (Ta) as well as indium tin oxide (ITO) as a novel current collector, stable up to 2.75 V vs. Al. More importantly, Chen et al. [31] describe platinum (Pt) as well as Mo to oxidize at 1.8 V and 2 V in AlCl₃-EMImCl, 1.3:1 ratio, electrolyte. However, no further effort has been made to investigate the redox activity of Mo and its influence on the electrochemical performance. Nearly the same redox behavior (1.85 V and 1.98 V vs. Al) is shown for Mo by Yu et al. [32] but like a lot of other authors, they use Mo foil as a current collector, since they falsely assumed the activity would be negligible. In the present report, the actual influence of side reactions between the Mo current collector and the AlCl₃-based ionic liquid electrolyte and on the electrochemical performance of RABs is demonstrated. In addition, it was possible to show that a coated layer of an inactive Co₃O₄, initially supposed to be an active material [33], hampers the reaction of the Mo current collector with the electrolyte.

2. Materials and methods

2.1. Synthesis of cathode material

For the synthesis of 1.00 g pure Co₃O₄ cathode material, a typical hydrothermal method has been used. 1.03 g cobalt acetate tetrahydrate

($\text{Co}(\text{CH}_3\text{COO})_2 \times 4\text{H}_2\text{O}$, 4.15 mmol) were dissolved in a 250 ml beaker with 60 ml deionized water. 80 mg hexadecyltrimethylammonium bromide (CTAB, $(\text{CH}_3(\text{CH}_2)_{15}\text{N}(\text{CH}_3)_3$, 0.22 mmol) were added to the solution as a surfactant. Afterwards, 0.25 mg urea ($\text{CO}(\text{NH}_2)_2$, 4.14 mmol) were added to the solution. The clear pink solution was transferred into a Teflon-lined stainless-steel autoclave (100 ml capacity, PARR INSTRUMENT COMPANY) and sealed. Then, the hydrothermal synthesis was carried out in a drying and heating oven (BINDER) at 160 °C for 20 h. After the heating process, the reaction vessel was allowed to cool down to room temperature. A pink solid was obtained, which was separated *via* filtration from the solution and was then washed several times, first with deionized water, followed by absolute ethanol. The solid intermediate product was stored overnight at 60 °C in an oven for drying. Finally, the dry solid was transferred into a porcelain crucible and it was heated in ambient atmosphere at 500 °C for 4 h in a muffle oven. The obtained product was a black powder, which was characterized *via* XRD, FT-IR and Raman as a pure Co_3O_4 compound.

2.2. Electrodes preparation

The electrodes were prepared by mixing 80 mass-% (400.0 mg) cubic Co_3O_4 material, 10 mass-% (50.0 mg) C65 carbon additive and 10 mass-% (500.0 mg) polyvinylidene fluoride (PVdF) binder (10 mass-%) dissolved in dimethyl sulfoxide (DMSO), in a DAC 150.1 FVZ SPEED-MIXER™ by HAUSCHILD. For slurry preparation, Co_3O_4 powder and C65 carbon were mixed and ground in a mortar with a pestle. The powders were dry mixed in the SpeedMixer at 1000 rpm for 2 min. Afterwards, two drops of DMSO were added and mixed with the powder at 2500 rpm for 2 min. The addition of DMSO was repeated three times until a homogeneous paste was obtained. Next, the slurry was sonicated for 5 min to achieve good homogeneity and less agglomeration. Then, PVdF binder solution was added and speed-mixed at 800 rpm for 10 min. The obtained suspension was coated with the doctor-blade technique on molybdenum (Mo; 99.9 % purity, 0.025 mm thickness, GoodFellow) foil using a ZUA200 doctor blade from ZEHNTNER (on a Coatmaster 510 Film Applicator from ERICHSEN with automatic feed), with a wet thickness of 100 μm . The coated Mo foil was dried under ambient conditions overnight. After that, the electrodes were dried in an oven at 60 °C for 6 h. Finally, the electrodes were punched out into 12 mm diameter discs (1.131 cm^2) and dried in a glass oven (BÜCHI Glass Oven B-585) in a vacuum at 120 °C for 12 h and then they were transferred into a Glovebox. The average mass of Co_3O_4 material on the electrodes was $0.73 \pm 0.09 \text{ mg cm}^{-2}$. The same procedure has been done to prepare electrodes with Mo-powder (99.95 % purity, 4–8 μm particle size, Sigma Aldrich). For these electrodes, tungsten (W; 99.96 % purity, 0.025 mm thickness, GoodFellow) was used as the current collector instead of a Mo-foil. The adhesion between both metals was weak and the electrodes needed to be handled carefully. The average mass of the Mo-powder on the electrodes was $1.29 \pm 0.16 \text{ mg cm}^{-2}$.

2.3. Electrolyte preparation

The electrolyte for electrochemical measurements was prepared inside a Glovebox, filled with inert Argon (Ar) gas and a water (H_2O) and oxygen (O_2) level of <0.1 ppm. The Lewis acidic ionic liquid electrolyte consists of 1-ethyl-3-methylimidazolium chloride (EMImCl) and aluminum chloride (AlCl_3) in the molar ratio of 1:1.5. The ionic liquid was prepared by slow addition of 4.00 g AlCl_3 (30 mmol) to 3.09 g EMImCl (21.07 mmol) while stirring. It was necessary to combine both components slowly by adding only a small amount of AlCl_3 because the formation of the ionic liquid is an exothermic reaction. After the complete addition, the liquid was stirred for further 24 h. The resulting electrolyte was colourless/yellowish.

2.4. Cell assembly and electrochemical characterization

The PFA Swagelok cells, whose pistons are made of Mo, were arranged in a two-electrode configuration for electrochemical measurements. The aluminum (Al; 99.0 % purity, 0.025 mm thickness, GoodFellow) anode is used as both, a reference and counter electrode. The cathode electrode discs were punched out with a manual punching machine GN-CP20 from GELON GROUP. The pure aluminum anode electrode discs (12 mm) and separator (13 mm) were punched out with a TURNUS bracket hollow. Each cell part of the Swagelok cell was dried overnight at 120 °C in a drying and heating oven from BINDER and inserted afterwards into an Ar-filled Glovebox from MBRAUN with an O_2 and H_2O level less than 0.5 ppm to assemble the cells. A 12 mm diameter coated working electrode was placed in the cell followed by a 13 mm diameter vacuum dried inside a BÜCHI glass oven B-584 glass-fiber separator (GF/D from WHATMAN®). Then 200 μl of EMImCl- AlCl_3 (1:1.5) ionic liquid was added and covered with a second separator and the same amount of electrolyte was added. The counter/reference aluminum electrode was placed on top of the second separator. All electrochemical measurements (GCPL with a current density of 20 mA g^{-1} and CV with a scan rate of 0.5 mV s^{-1} in the potential window of 0.3 V–2.2 V) were carried out using a VMP3 multichannel potentiostat/galvanostat from BIO-LOGIC SCIENCE INSTRUMENTS (France), equipped with the EC-Lab software.

2.5. Characterization techniques

2.5.1. X-ray diffraction (XRD)

XRD diffractograms of the Co_3O_4 compound were recorded in glass no. 50 capillaries from Hilgenberg at room temperature using an X-ray powder diffractometer from STOE STADI P. The device operates with $\text{Mo K}\alpha_1$ radiation ($\lambda = 0.7039 \text{ \AA}$). All diffraction patterns were analyzed by full-pattern Rietveld refinements, using the software package FullProf [34] and plotted with Origin2023 from ORIGINLAB.

2.5.2. Scanning electron microscopy (SEM)

SEM investigations were conducted by a thermal field emission scanning electron microscope (FESEM, Carl Zeiss SMT AG) at an acceleration voltage of 5 kV. The samples were fixed on a steel sample holder by using adhesive tape.

2.5.3. Inductively coupled plasma – optical emission spectroscopy (ICP-OES)

ICP-OES was performed by a OPTIMA 4300DV (PerkinElmer) with an Echelle polychromator and a solid-state detector (custom, two-dimensional CCD array). Before the ICP-OES measurement, all samples were dissolved in *aqua regia* (hydrochloric acid: nitric acid in the ratio 3:1, respectively).

2.5.4. Raman spectroscopy

Raman active modes were measured by a Raman spectrometer (LabRam, Evolution HR, HORIBA Jobin Yvon) with 633 nm laser excitation wavelength in a range from 100 to 4000 cm^{-1} . Data evaluation was done with Origin2023 from ORIGINLAB.

2.5.5. Fourier-transform infrared (FT-IR)

FT-IR active vibrations were measured with a Bruker Tensor 27 FTIR spectrometer. Data evaluation was done with Origin2023 from ORIGINLAB.

2.5.6. X-ray photoelectron spectroscopy (XPS)

XPS measurements were performed using a K-Alpha XPS spectrometer from Thermo Fisher Scientific (East Grinstead). The samples were irradiated with monochromatic Al- $\text{K}\alpha$ X-rays with a spot size of about 400 μm . The photoelectrons were detected with a hemispherical 180 dual-focus analyzer with 128 channel detectors. To prevent any

localized charge buildup, the $K\alpha$ charge compensation system was employed during analysis, using electrons of 8 eV energy and low-energy argon ions. The samples were fixed on a steel sample holder by using Cu-based adhesion tape. For data evaluation, Avantage 5.9925 Surface Chemical Analysis software from Thermo Fischer Scientific was used.

2.5.7. Ball mill

The grinding of the Co_3O_4 has been done with a Fritsch Pulverisette 7 using ZrO_2 jars and milling balls. The ball milling was done for 16 h at 500 rpm (revolutions per minute) under argon atmosphere. After every 10 min of grinding, the ball milling was stopped for 5 min to avoid too high temperatures and structural destruction or decomposition.

2.5.8. Hydrogen and carbon nuclear magnetic resonance (^1H - and ^{13}C -NMR)

^1H - and ^{13}C -NMR spectra have been recorded with a Bruker Avance 400 spectrometer with an applied frequency of 400 MHz and 101 MHz,

respectively. As a solvent, d6-acetone ($(\text{CD}_3)_2\text{CO}$; 99.9 atom% D, Sigma-Aldrich) has been used. Data evaluation was done with MestReNova from Mestrelab Research, software version 14.1.2–25024.

2.5.9. Magnetometry

Direct current (DC) magnetometry data has been measured with a Physical Property Measurement System (PPMS) DynaCool from Quantum Design equipped with a Vibrating Sample Magnetometry (VSM) option. The magnetic moment was measured from 2 to 160 K at a magnetic field of 5 kOe with an average signal acquisition time per measuring point of 10 s for all samples. Liquids were measured in a custom-made sample container based on magnetically clean drinking straws (QDS-8000-001 from Quantum Design). To prepare 100 mg of the red-coloured electrolyte consisting out of (partially) dissolved Mo and $\text{AlCl}_3\text{:EMImCl}$, 7.165 mg Mo metal were immersed for 72 h in 92.836 mg clean electrolyte. 100.3(1) mg of such red-coloured electrolyte with immersed Mo was measured and the raw magnetic moment (emu) was normalized to 100 mg (that would contain 7.165 mg Mo) and to a

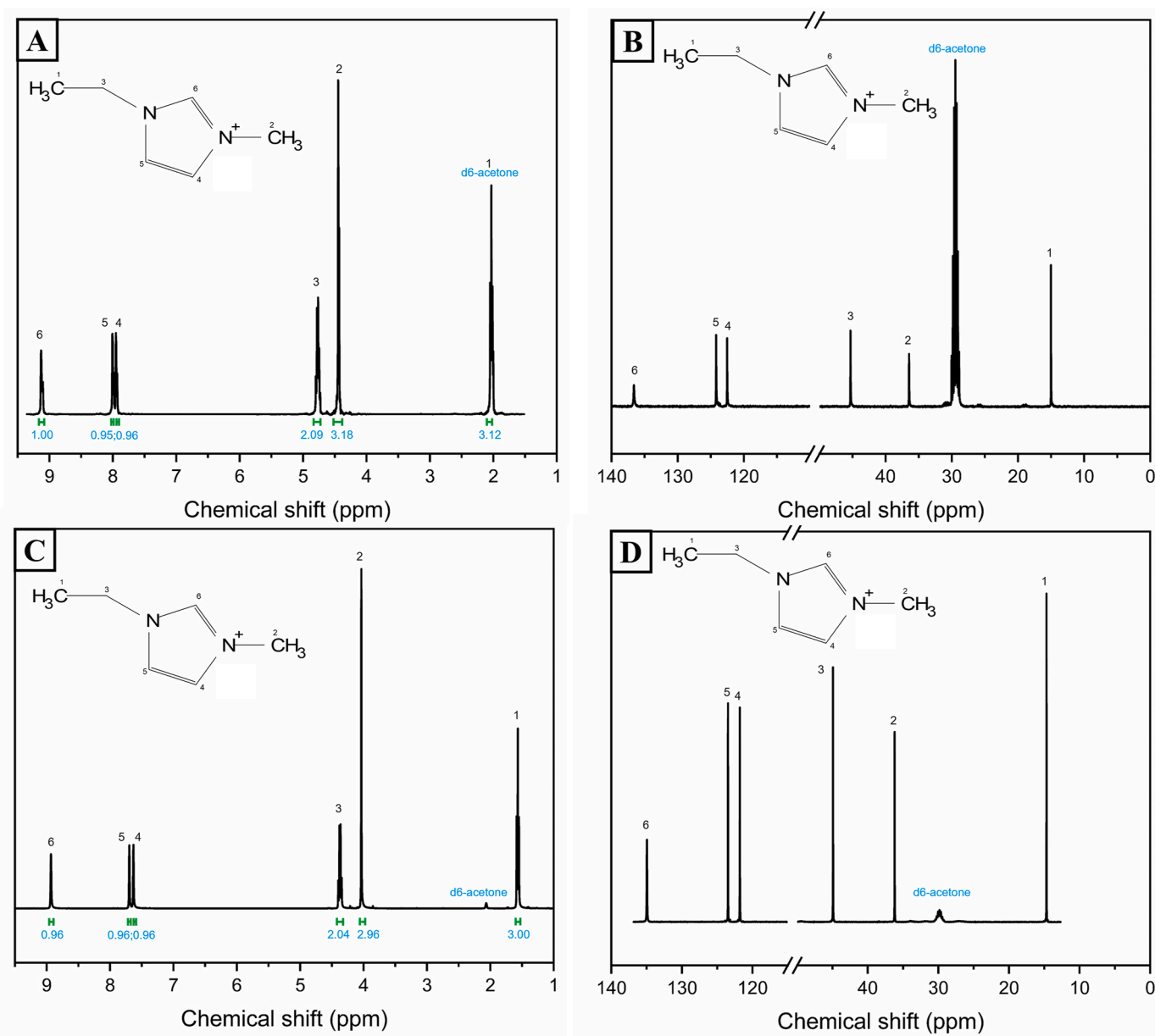


Fig. 1. ^1H - and ^{13}C -NMR of freshly prepared $\text{AlCl}_3\text{-EMImCl}$ electrolyte (A, B) and ^1H - and ^{13}C -NMR of red $\text{Mo-AlCl}_3\text{-EMImCl}$ (C, D), respectively. (For interpretation of the references to colour in this figure legend, the reader is referred to the Web version of this article.)

magnetic field of one Oe. Further, 156.2 mg of the pure electrolyte (without Mo) were measured and the raw magnetic moment was normalized to 92.835 mg and to a magnetic field of one Oe. The magnetic contribution stemming exclusively from the 7.165 mg of immersed Mo (blue symbols in Fig. 2) has been obtained by subtracting the signal from the pure electrolyte (orange symbols in Fig. 2) from the signal of the electrolyte with the immersed Mo (red symbols in Fig. 2). For comparison, Mo metal powder (38.5 mg) and Mo-foil (31 mg) were measured within polypropylene sample capsules (QDS-4096-388 from Quantum Design) and the measured raw data magnetic moment have been normalized to 7.165 mg and to a magnetic field of one Oe.

3. Results and discussion

After immersion of Mo-foil or powder with a bigger surface area (4–8 μm particle size), the colourless/yellowish $\text{AlCl}_3\text{-EMImCl}$ (1.5:1) ionic liquid electrolyte turns red after a few seconds. This is the first indication that side reactions take place, leading to the formation of Mo-cations that can form complexes with the AlCl_3 -based ionic liquid. For clarity, in the following, in Lewis acidic electrolyte immersed Mo will be labelled as Mo- $\text{AlCl}_3\text{-EMImCl}$. Only a few authors, such as Chen et al. [31], who presented an indium tin oxide (ITO)-based current collector, mention a side effect of Mo to occur. However, in their report, the oxidation of Mo is explained to occur due to the residual amount of water in the electrolyte. To ensure that the ionic liquid used in this work is water-free, ^1H - and ^{13}C -NMR spectroscopy has been done. Fig. 1 A and B show the ^1H - and ^{13}C -NMR of freshly prepared $\text{AlCl}_3\text{-EMImCl}$ ionic liquid. All signals of both spectra can be assigned to the EMIm^+ cation. No hydrogen water peak at 2.84 ppm is visible before (Fig. 1 A) and after the immersion of Mo (Fig. 1 C). Since no signal appears, it can be assumed that the residual water amount is below the detection limit ($0.01 \text{ mol}\cdot\text{kg}^{-1}$ or 0.02 mass-%) [35]. Fig. 1 C and D show the ^1H - and ^{13}C -NMR measurements of the red Mo- $\text{AlCl}_3\text{-EMImCl}$.

Both NMR spectra (Fig. 1 C and D) prove that no structural change of the EMIm^+ happens. Furthermore, no significant chemical shift change occurs for the carbon atoms of the EMIm^+ . On the other hand, a slight upfield shift (~ 0.5 ppm) of all ^1H signals occurs for the Mo- $\text{AlCl}_3\text{-EMImCl}$ sample. This phenomenon can be caused by an increased electron density around the hydrogen atoms due to the presence of metal

cations. The increased electron density shields the hydrogen nucleus from the external magnetic field, resulting in an upfield shift [36]. Similar NMR results have been obtained for an EMImCl-PbCl_2 system by Tan et al. [37], where $[\text{Pb}_m\text{Cl}_{2m+1}][\text{EMImCl}]_n$ ($m = 1, 2$ and $n = 1-4$) clusters or complexes have been formed. It should be noted that this Pb-Cl-EMImCl investigation has been done without the addition of AlCl_3 . However, it is possible that molybdenum dissolves in the ionic liquid and forms similar complexes or clusters. Inductively coupled plasma optical emission spectroscopy (ICP-OES) confirmed that in 5 mg saturated Mo- $\text{AlCl}_3\text{-EMImCl}$ electrolyte, it was possible to dissolve 1.99

± 0.06 mass-% of Mo. It should be noted that any remaining Mo nanoparticles that stay unfiltered can distort the ICP-OES result. Based on the result of ICP-OES, temperature-dependent magnetic susceptibility χ measurements have been performed. As shown in Fig. 2, the pure $\text{AlCl}_3\text{-EMImCl}$ ionic liquid electrolyte exhibits temperature-independent Langevin diamagnetism over almost the whole investigated temperature range from 160 K down to approximately 10 K. Below 10 K, the electrolyte is supposed to undergo a phase transition with an accompanying increase of electron density and corresponding stronger diamagnetic signal. On the other side, Mo metal (measured here as Mo-foil and powder, respectively) only exhibits a weak positive temperature-independent Pauli paramagnetism over the whole temperature range. When Mo metal powder has been immersed and stirred for 72 h in $\text{AlCl}_3\text{-EMImCl}$ (1.5:1) ionic liquid electrolyte, the susceptibility increases strongly when the temperature is lowered as it is characteristic for Langevin-type paramagnetism of localized magnetic moments. The magnetic susceptibility that exclusively stems from the (partially) dissolved Mo can be obtained by subtracting the signal contribution of the pure electrolyte from that of the Mo immersed in the electrolyte (see experimental section for details). A Curie-Weiss fit (inset in Fig. 2) according to $\chi^{-1} = C^{-1}(T - \theta)$, with the Curie constant C , and the Weiss constant θ , has been done from 2 to 150 K. Referring to the total amount of Mo atoms contained in 7.165 mg Mo, a molar Curie constant of $C_{\text{mol}} = 2.70(1) \cdot 10^{-2} \text{ cm}^3\cdot\text{K}\cdot\text{mol}^{-1}$ is obtained that corresponds to a localized paramagnetic moment of $0.47(1) \mu_{\text{B}}$ per Mo atom on average. Alternatively, the Curie constant could also be explained by approximately 8 % of all Mo atoms exhibiting a single unpaired electron with paramagnetic moment of $1.73 \mu_{\text{B}}$. The obtained small negative Weiss-constant of $\theta = -2.7(4)$ K points either to a realized weak anti-ferromagnetic coupling between the Mo magnetic moments in a multi Mo containing complex and/or to weak single-ion anisotropy [38].

Misirlioglu and Aksüt [39] demonstrated the formation of $[\text{MoOCl}_4]^-$ depending on the Cl $^-$ concentration in a HCl solution, and $[\text{MoOCl}_4]^-$ is paramagnetic [40]. On the other hand, the formation of solvable $\text{Mo}^{(\text{II-VI})}\text{Cl}_{(2-6)}$ complexes are also possible. Estager et al. [41] show in their review article from 2014 that such dissolution behavior of metal chlorides, like CoCl_2 , NiCl_2 , FeCl_2 , FeCl_3 , CuCl_2 , MoCl_3 , and MoCl_4 , in basic chloroaluminate ionic liquid is possible. UV-VIS spectra (Fig. 3 A and B) of the red Mo- $\text{AlCl}_3\text{-EMImCl}$ electrolyte have been recorded to get more information about potentially formed Mo cations. For dilution of the liquid sample, 1,2-Difluorobenzene (DFB) has been chosen since the solvent does not react with the ionic liquid and does not overlap with the UV-VIS bands of the red electrolyte with dissolved Mo cations. (Fig. 3 A).

It was not possible to obtain two bands for the pure ionic liquid electrolyte (Fig. 3 A and B, red line). Three reasons can be given for these bad signals, which are supposed to occur at 305 nm and 368 nm [42]. First of all, the samples were oversaturated. Secondly, the measurements have been done at room temperature. At elevated temperature, absorbance and splitting would be favored. Thirdly, EMIm^+ , AlCl_4^- and Al_2Cl_7^- have a lack of UV-VIS active chromophores. Lang et al. [42] demonstrated that a concentration of $6.8 \text{ mM}\cdot\text{L}^{-1}$ of $\text{AlCl}_3\text{:EMImCl}$ (2:1), diluted with dichloro methane (CH_2Cl_2) and the UV-VIS spectra will result in a sufficient splitting of the IL bands with relatively high absorbance at a temperature in the range of $40 \text{ }^\circ\text{C}$ – $100 \text{ }^\circ\text{C}$. After the reaction of the Mo

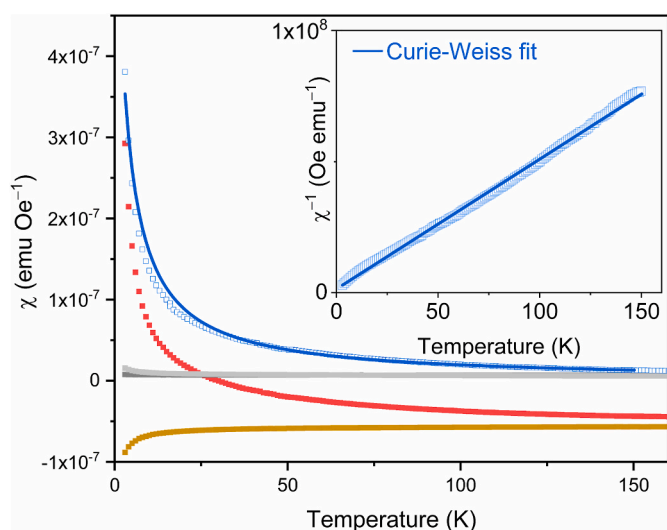


Fig. 2. Magnetic DC susceptibility vs. temperature of Mo- $\text{AlCl}_3\text{-EMImCl}$ (red), pure electrolyte (orange), metal Mo-foil (dark grey), and Mo-powder (light grey), Langevin-type paramagnetic contribution stemming from the immersed Mo (blue), and Curie-Weiss fit (blue solid line). Inset shows inverse DC susceptibility vs. temperature plot. (For interpretation of the references to colour in this figure legend, the reader is referred to the Web version of this article.)

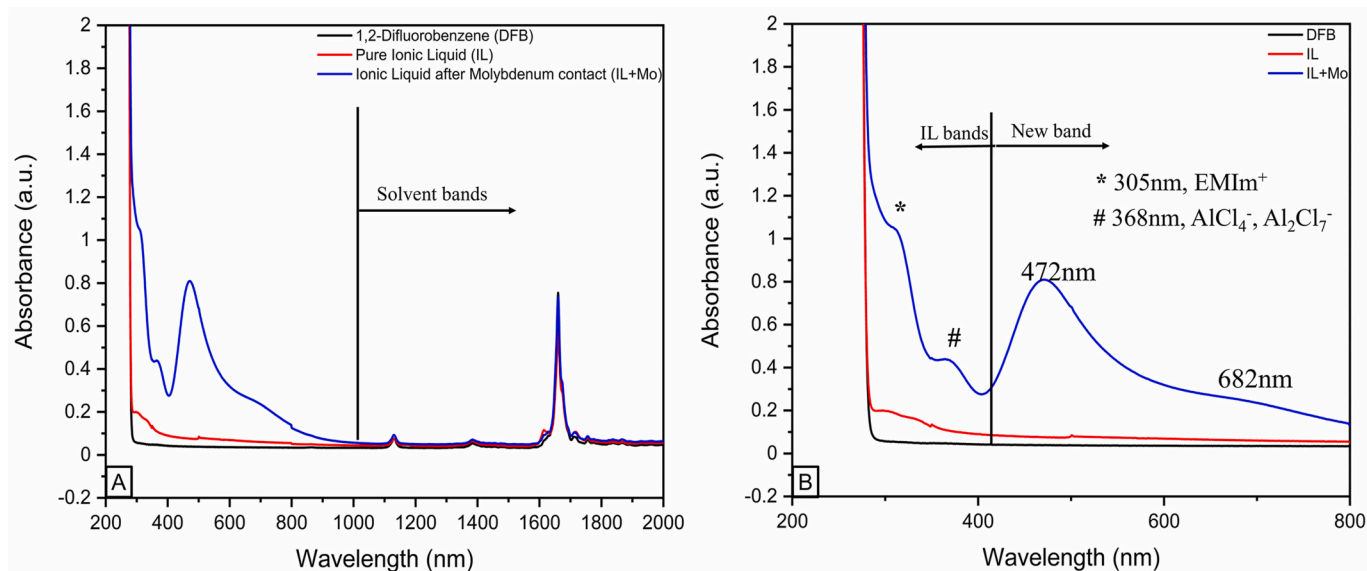


Fig. 3. Ultraviolet–Visible (UV–VIS) spectra (A) of the whole wavelength range (200–2000 nm), and (B) in the range of 200–800 nm with occurring bands of the ionic liquid, marked with an asterisk (*) and a hash (#) and newly arising bands.

with the ionic liquid (Fig. 3 B, blue line) a new Mo-AlCl₃-EMImCl related band at 472 nm (blue wavelength area) and a shoulder around 682 nm (red wavelength area) appear. Hartmann and Schmidt [43] reported similar results of absorption spectroscopy of molybdenum(III)-chlorides in acidic solutions. In addition, Scheffler et al. [44] published comparable results of solvated Mo³⁺ and Mo⁴⁺ chloro complexes in AlCl₃:EMImCl (1.3:1) ionic liquid environment. Therefore, it is expected that the dissolution of the Mo metal in the Lewis acidic electrolyte leads to the formation of Mo³⁺ and Mo⁴⁺ chloro complexes. It was possible to prove via ICP-OES, UV–VIS and temperature-dependent magnetic susceptibility measurements, that the instability of metallic Mo in Lewis acidic AlCl₃:EMImCl ionic liquid electrolyte leads to the dissolution of Mo. This finding raises the question to what extent the Mo instability influences electrochemical measurements. Chen et al. [31] describe the electrochemical oxidation of Mo to be similar to platinum (Pt), whereby both metals show an onset oxidation peak at 1.8 V (vs. Al), measured via linear sweep voltammetry (LSV) with an AlCl₃-EMImCl (1.3:1) electrolyte. A similar activity of Mo has been reported by Yu et al. [32]. By

running cyclic voltammetry (CV) measurements, the oxidation of Mo at 1.85 V and 1.98 V (vs. Al) could be recorded with an AlCl₃-1-butyl-3-methylimidazolium chloride (BMICl) electrolyte in the molar ratio 1.6:1 [33]. However, Yu et al. [32] explain the reactivity of Mo to be negligible, compared to the contribution from the graphite positive electrode. Nevertheless, while evaluating the electrochemical activity of novel promising materials, the redox reactions and related specific capacity may be misled by the Mo side reaction with the Lewis acidic electrolyte. Moreover, to prove the stability of Mo, most reported investigations show only one LSV or one CV cycle, without considering a possible activation of the system, which may take several cycles [30]. Therefore, a cyclic voltammogram of pure Mo-foil (Fig. 4 A) and ball-milled Co₃O₄ coated on a Mo-foil (Fig. 4 B) at a scan rate of 0.5 mV s⁻¹ have been recorded against an Al anode. Co₃O₄ has been chosen because Liu et al. [33] reported this material to be an excellent positive electrode material for RABs, with an initial discharge capacity of 490 mAh g⁻¹ at a current density of 50 mA g⁻¹.

Both CVs, with and without Co₃O₄ material on the Mo-foil show

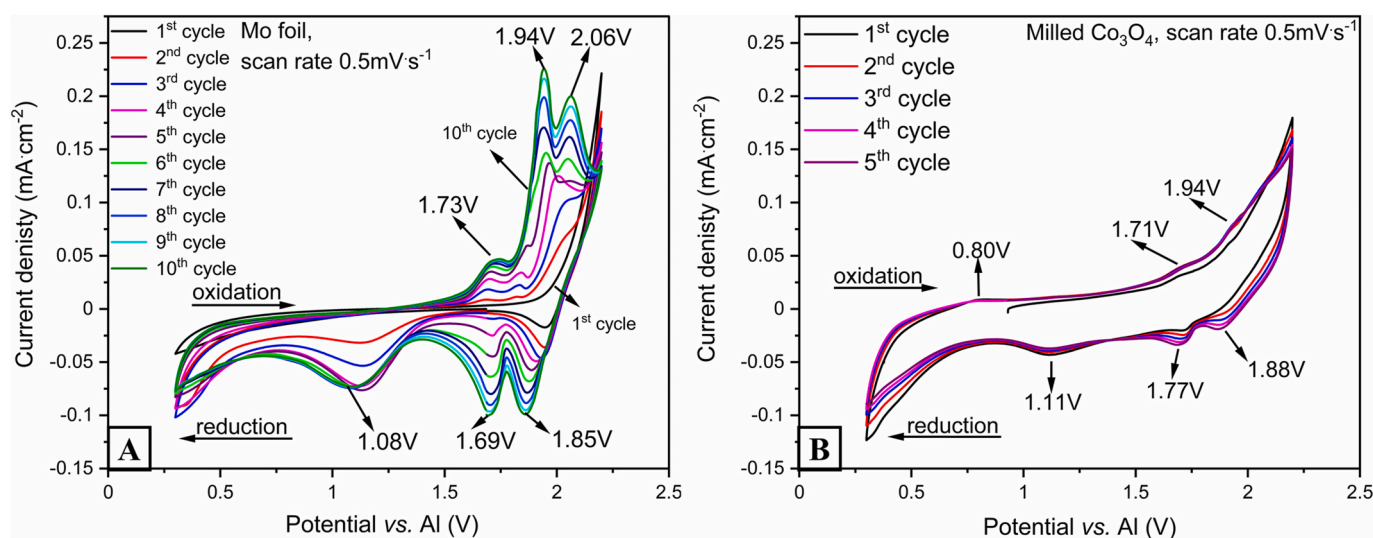


Fig. 4. Cyclic voltammograms (CVs) of pure Mo-foil (A) and milled Co₃O₄ (B) that was coated on a Mo-foil at a scan rate of 0.5 mV s⁻¹ in a potential window of 0.3 V–2.2 V.

similar redox peak positions. Pure Mo-foil (Fig. 4 A) shows three reversible oxidation (1.73 V, 1.94 V and 2.06 V) and reduction (1.85 V, 1.69 V and 1.08 V) peaks, whose intensity increases with an increasing number of cycles. The redox activity recorded on the Mo-foil has a predominant influence on the electrochemical signature and the rising current density is due to the longer reaction time. Co_3O_4 coated on Mo-foil (Fig. 4 B) shows redox activity at the same potentials and an additional small oxidation peak around 0.80 V, which belongs to the oxidation of the Co-based spinel and is comparable with the results of Liu et al. [33]. Certainly, the redox activity of the Co_3O_4 material is rather small. The intensity of the Mo peaks in Fig. 4 B are lower because of the “protective” layer of coated quasi-inactive Co_3O_4 . The reactive surface area of Mo is much more reduced compared with that of the pure Mo-foil. Since the dissolution of Mo takes place already after the contact with the electrolyte, it can be assumed that the previous AlCl_4 , Al_2Cl_7 , EMIm^+ compounds are not anymore responsible for the occurrence of redox activity, but newly formed Mo cation-based complexes or clusters in combination with the IL. Yu et al. [32] describe the identical redox behaviour of the Mo-foil current collector but report the redox activity would be negligible. Similar results, like those obtained by Yu et al. [32] and shown in this work, were published by Sun et al. [45], who describe the redox behaviour just to be an interface reaction between Mo and the electrolyte. However, a solid-liquid interface reaction does not lead to the dissolution of the electrode, like it is shown with Mo- AlCl_3 -EMImCl in this work. Such instabilities of metallic cell parts can lead to significant false discharge capacities from 150 mAh g^{-1} to 400 mAh g^{-1} and can be misleading when characterising novel electrode materials [46]. To prove the specific capacity contribution from molybdenum side reactions, galvanostatic cycling with potential limitation (GCPL) has been done with Mo powder, coated on a tungsten (W) current collector. Tungsten has been chosen as the current collector because it is considered stable in IL electrolytes [28]. Fig. 5 A shows the GCPL of Mo-powder at a current density of 20 mA g^{-1} in the potential window from 0.3 V to 2.2 V and Fig. 5 B the corresponding coulombic efficiency of the charge (blue)/discharge (red) curves.

During the first charge cycle (Fig. 5 A, black curve), a long oxidation plateau occurs around 1.75 V, which corresponds to the first oxidation peak in the CV of the Mo-foil. Due to parasitic side reactions, the potential shows instability until it reaches the upper limit of 2.2 V. Especially during the first 10 cycles, the influence of the side reactions seems to have the biggest influence on the electrochemical performance. An indication of this assumption is that the coulombic efficiency is above 100 % (Fig. 5 B) and falls below 100 % after 40 cycles. For a certain time,

the Mo-powder cell delivers a relatively stable discharge capacity of $\sim 60 \text{ mAh g}^{-1}$ before the capacity started to increase again to reach a discharge capacity of $\sim 136 \text{ mAh g}^{-1}$ at a rate of 20 mA g^{-1} after 100 cycles. It is also worth mentioning that the GCPL measurement of the Mo-powder collapses after 125 cycles. In total, the capacity increase over cycling and the evolution of the CE could be due to the following processes occurring in three steps; I) The initiation of the parasitic side reaction between Mo and the AlCl_3 :EMImCl (1.5:1) ionic liquid electrolyte during the first 10 cycles. During the initial cycles, most possible side- and activation reactions occur and lead to a CE $>100 \%$. II) Until the 40th cycle, charge and discharge are in a steady-state (ss) process with a stable CE. III) After the 40th cycle, side reactions are more pronounced during the oxidation/corrosion/dissolution process at the positive electrode causing a continuous decrease of the CE. It is assumed that after the second stage, the dissolution of Mo becomes the main reaction, providing more Mo-based redox active species. Diem et al. [47] obtained similar results for the dissolution of copper (Cu) in AlCl_3 :EMImCl (1.5:1) ionic liquid electrolyte. Based on the Mo- AlCl_3 -EMImCl results, an additional indication of the proposed Mo-chloro complexes is the similarity with a tellurium (Te) metal system, which got dissolved in AlCl_3 :EMImCl (1.3:1) ionic liquid electrolyte [48]. After adding Te powder to the AlCl_3 -based electrolyte, Zhang et al. [48] describe the formation of AlTeCl and $\text{TeCl}_3\text{AlCl}_4$, which resulted in a color change of the ionic liquid from light-yellow to red-brown. Furthermore, a dissolution and electrochemical redox cycle for the metallic Te positive electrode has been proposed, leading to Te(II) and $\text{Te(IV}^+)$ formation out of Te(0) [48]. The high redox ability of Te in a Lewis acidic ionic liquid electrolyte leads to the formation of an active tellurium chloroaluminate compound which delivers an initial discharge capacity of $\sim 1026 \text{ mAh g}^{-1}$ at a rate of 0.5 A g^{-1} [48]. Since molybdenum can reach the same oxidation states (II to VI⁺) as tellurium, it is expected that the performance of both metals can be compared. An indication of the similarity concerning the dissolution characteristics between Mo and Te can be seen from the obtained X-ray photoelectron spectroscopy (XPS) results (Fig. 6 B). Since Mo gets dissolved and interacts with the ionic liquid electrolyte, a shuttle effect of Mo-ions to the cycled aluminum negative electrode occurs. A similar migration effect has been reported by Reed et al. [6] in the case of using a current collector and cell body made out of SS. As an explanation, it is mentioned that FeCl_2 and CrCl_2 can undergo a reduction reaction with Al and AlCl_4 (Eq. I and II), which results in iron and chromium metals. Fig. 6 A, shows the XPS survey of pure Al negative electrode. Besides the typical Al 2p and O 1s (and Al-O) signals, a Cl 2p peak is visible due to the chlorine-containing

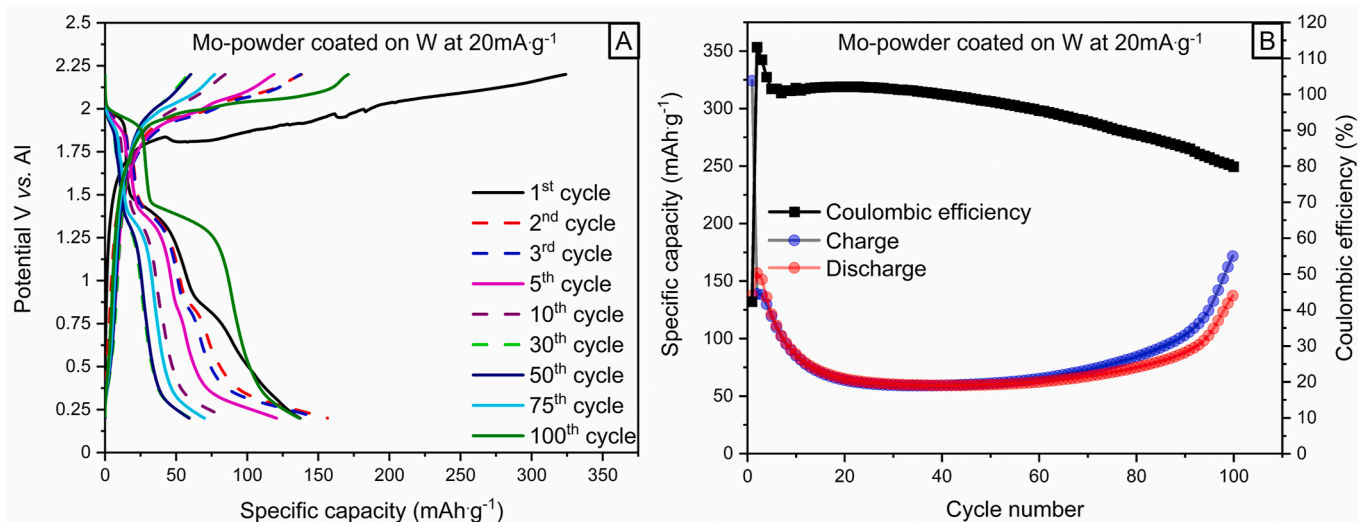


Fig. 5. Galvanostatic cycling with potential limitation (GCPL) of Mo-powder coated on W-foil in the potential window 0.3 V–2.2 V at a current density of 20 mA g^{-1} (A) and the corresponding charge/discharge graph, including the coulombic efficiency (B).

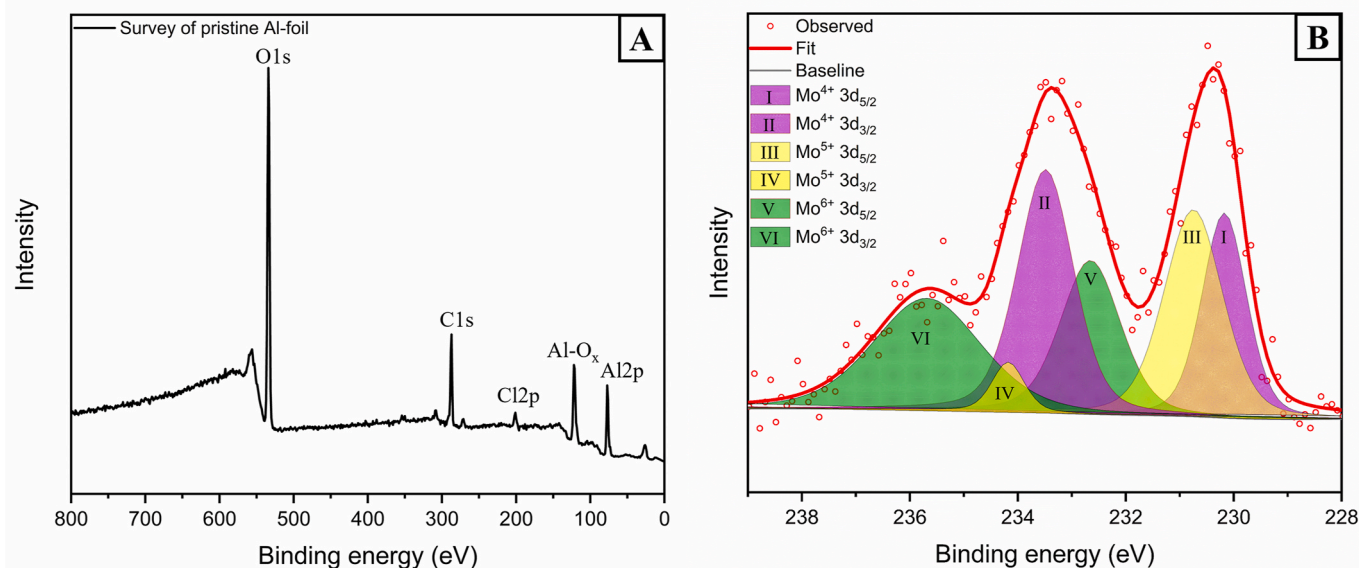


Fig. 6. X-ray photoelectron spectroscopy (XPS) survey of pristine Al-foil (A) and XPS spectra of $\text{Mo}^{4+/5+/6+}$ cations on Al-foil (B) stopped at 0.3 V.

environment inside the Glovebox caused by the $\text{AlCl}_3\text{:EMImCl}$ electrolyte. However, no Mo signals in the region from around 236 to 230 eV (Fig. 6 A) can be detected. Fig. 6 B shows the XPS spectra of Mo^{4+} , Mo^{5+} , and Mo^{6+} on an Al negative electrode stopped after complete discharge at 0.3 V. After fitting, peaks at (VI $\text{Mo}^{6+} 3d_{3/2}$) 235.68 eV, (IV $\text{Mo}^{5+} 3d_{3/2}$) 234.18 eV, (II $\text{Mo}^{4+} 3d_{3/2}$) 233.48 eV, (V $\text{Mo}^{6+} 3d_{5/2}$) 232.68 eV, (III $\text{Mo}^{5+} 3d_{5/2}$) 230.78 eV, and (I $\text{Mo}^{4+} 3d_{5/2}$) 230.18 eV are obtained, which can be assigned to the oxidation states of Mo^{4+} (purple peaks), Mo^{5+} (yellow peaks), and Mo^{6+} (green peaks). However, metallic Mo is not present since the Mo $3d_{5/2}$ electron binding energy at 228 eV is missing. The oxidation states of Mo probably belong to several kinds of Mo-O layers. An indication for this assumption is that the two peaks at lower binding energies are symmetrical, while the peaks appear asymmetrical in the case of Mo metal.

Since the peaks with binding energies at 235.68 and 232.68 eV are characteristic for MoO_3 [49], it is assumed that this Mo-oxide has formed. A similar formation of a metal oxide layer has been reported for metallic Ni current collector used in an $\text{AlCl}_3\text{:EMImCl}$ (1.3:1) electrolyte RAB system [27]. It has been shown that Ni used as a current collector forms an oxide layer consisting of NiO and Ni_2O_3 [27] as well and can, therefore, be compared with the Mo system. In contrast to the Mo-Al- $\text{AlCl}_3\text{:EMImCl}$ results of the UV-VIS spectroscopy, it was not possible to detect the Mo^{3+} oxidation state, via XPS. A reasonable explanation could be that the proposed Mo^{3+} -chloro compound is only stable in ionic liquid electrolytes. If MoCl_x^+ compounds are formed during the reaction between Mo and $\text{AlCl}_4^-/\text{Al}_2\text{Cl}_7^-$, these Mo-compounds can perform a hydrolysis and oxidation reaction [50] after removing the sample from the electrolyte. Even a small amount of H_2O can initiate an oxidation of Mo^{3+} , resulting in higher Mo^{x+} ($x = 4, 5, 6$) oxidation states.

To sum up, several observations clearly indicate that the molybdenum, used as the current collector, is unstable and undergoes a reaction with the $\text{AlCl}_3\text{:EMImCl}$ (1.5:1) ionic liquid electrolyte. One indication of a dissolution and complex formation is the change of the electrolyte color from colourless/yellowish to red after getting in touch with a Mo source. UV-VIS measurements of the red Mo-Al $\text{AlCl}_3\text{:EMImCl}$ ionic liquid show newly occurring non-electrolyte-related bands, which usually appear for Mo^{3+} and Mo^{4+} ions. Moreover, in comparison to the fresh mixed ionic liquid, the electrolyte after reacting with Mo exhibits Langevin-type paramagnetism from localized magnetic moments as present in Mo-complexes or also -oxides for instance, whereas metallic Mo would only exhibit temperature-independent Pauli paramagnetism.

ICP-OES tests confirm a dissolution of Mo of 1.99 ± 0.06 mass-% in 5 mg ionic liquid electrolyte. Cyclic voltammograms were recorded to understand the effect of Mo on the electrochemical reaction with $\text{AlCl}_3\text{:EMImCl}$ electrolyte. Oxidation peaks around 1.73 V, 1.94 V, and 2.06 V as well as reduction peaks at 1.85 V, 1.69 V, and 1.08 V, confirm that reversible reactions take place on the Mo electrode surface similar to Pt [31]. It is important to stress that, in the literature, the impact of Mo in AlCl_3 -based RABs is described to be negligible [32]. Instead, according to the results of this report, the entire capacity of $\sim 136 \text{ mAh g}^{-1}$ at a rate of 20 mA g^{-1} after 100 cycles, is due to the Mo side reactions. Furthermore, via XPS measurements it was possible to show that three different oxidation states of $\text{Mo}^{4+/5+/6+}$ exist on the Al negative electrode after running electrochemical tests. The Mo dissolves partly in the ionic liquid and shuttles to the anode. Mo^{3+} is supposed to be stable only in AlCl_3 -based ionic liquid electrolyte. Based on all shown results, it is assumed that Mo reacts similarly to tellurium and nickel to form Mo-Cl_x^+ and/or MoOCl_x^+ complexes.

4. Conclusion

All results suggest that the Mo current collector suffers from side reactions. The assumption that molybdenum shows redox activity due to residual water in the ionic liquid as reported in literature, could be discarded according to the results obtained in this work. The electrochemical oxidation of unstable metals can lead to significant false discharge capacities from 150 mAh g^{-1} to 400 mAh g^{-1} and be misleading when characterizing novel electrode materials. Therefore, it should be avoided to use Mo foil as a current collector and cell housing. Instead, anodic stable materials like carbon paper, glassy carbon, TiN, or ITO should be used for $\text{AlCl}_3\text{:EMImCl}$ ionic liquid-based RABs.

CRedit authorship contribution statement

Eugen Zemlyanushin: Writing – original draft, Visualization, Methodology, Investigation, Formal analysis, Data curation, Conceptualization. **Björn Schwarz:** Writing – review & editing, Visualization, Validation, Methodology, Investigation, Formal analysis, Conceptualization. **Sonia Dsoke:** Writing – review & editing, Supervision, Conceptualization.

Funding

This work contributes to the research performed at CELEST (Center of Electrochemical Energy Storage Ulm-Karlsruhe) and was funded by the German Research Foundation (DFG) under Project ID 390874152 (POLiS Cluster of Excellence, EXC 2154).

Declaration of competing interest

The authors declare that they have no known competing financial interests or personal relationships that could have appeared to influence the work reported in this paper.

Acknowledgments

The authors would like to thank Dr. Xinyue Li, Dr. Angelina Sarpulova, Prof. Noha Sabi, and Julian Hansen for helpful discussions and technical support.

Appendix A. Supplementary data

Supplementary data to this article can be found online at <https://doi.org/10.1016/j.jpowsour.2025.236458>.

Data availability

The data that support the findings of this study are available upon request.

References

- [1] F. Martins, C. Felgueiras, M. Smítková, N. Caetano, Analysis of fossil fuel energy consumption and environmental impacts in European countries, *Energies* 12 (6) (2019) 1–11, <https://doi.org/10.3390/en12060964>.
- [2] Y. Lyu, et al., An overview on the advances of LiCoO₂ cathodes for lithium-ion batteries, *Adv. Energy Mater.* 11 (2) (2021) 1–29, <https://doi.org/10.1002/aem.202000982>.
- [3] T.C. Wanger, The Lithium future-resources, recycling, and the environment, *Conserv. Lett.* 4 (3) (2011) 202–206, <https://doi.org/10.1111/j.1755-263X.2011.00166.x>.
- [4] G.A. Campbell, The cobalt market revisited, *Miner. Econ.* 33 (1–2) (2020) 21–28, <https://doi.org/10.1007/s13563-019-00173-8>.
- [5] L.A.W. Ellingsen, et al., Environmental screening of electrode materials for a rechargeable aluminum battery with an AlCl₃/EMIMCl electrolyte, *Materials* 11 (6) (2018), <https://doi.org/10.3390/ma11060936>.
- [6] L. Reed, UNIVERSITY OF CALIFORNIA, MERCED Aluminum Ion Batteries: Electrolytes and Cathodes, 2015.
- [7] D. Yuan, J. Zhao, W. Manalastas, S. Kumar, M. Srinivasan, Emerging rechargeable aqueous aluminum ion battery: Status, challenges, and outlooks, *Nano Mater. Sci.* 2 (3) (2020) 248–263, <https://doi.org/10.1016/j.nanoms.2019.11.001>.
- [8] T. Leisegang, et al., The aluminum-ion battery: a sustainable and seminal concept? *Front. Chem.* 7 (APR) (2019) 1–21, <https://doi.org/10.3389/fchem.2019.00268>.
- [9] N. Zhu, K. Zhang, F. Wu, Y. Bai, C. Wu, Review Article Ionic Liquid-Based Electrolytes for Aluminum/Magnesium/Sodium-Ion Batteries, vol. 2021, 2021.
- [10] E. Faegh, B. Ng, D. Hayman, W.E. Mustain, Practical assessment of the performance of aluminium battery technologies, *Nat. Energy* 6 (1) (2021) 21–29, <https://doi.org/10.1038/s41560-020-00728-y>.
- [11] Y. Hu, D. Sun, B. Luo, L. Wang, Recent progress and future trends of aluminum batteries, *Energy Technol.* 7 (1) (2019) 86–106, <https://doi.org/10.1002/ente.201800550>.
- [12] T. Schoetz, O. Leung, C.P. de Leon, C. Zaleski, I. Efimov, Aluminium deposition in EMIMCl-AlCl₃ ionic liquid and ionogel for improved aluminium batteries, *J. Electrochem. Soc.* 167 (4) (2020) 040516, <https://doi.org/10.1149/1945-7111/ab7573>.
- [13] J. Tu, et al., Nonaqueous rechargeable aluminum batteries: progresses, challenges, and perspectives, *Chem. Rev.* 121 (8) (2021) 4903–4961, <https://doi.org/10.1021/acs.chemrev.0c01257>.
- [14] D.M.-T. Castaño, Development and Optimization of Rechargeable Batteries Based on Aluminium, 2020, p. 231.
- [15] J. Yu, C. Liu, X. Hu, T. Wei, Y. Zhang, Z. Wang, A novel AlCl₃-[EMIM][TF2N] electrolyte for rechargeable aluminum-ion battery, *J. Phys. Conf. Ser.* 2044 (1) (2021), <https://doi.org/10.1088/1742-6596/2044/1/012048>.
- [16] G. Cohn, L. Ma, L.A. Archer, A novel non-aqueous aluminum sulfur battery, *J. Power Sources* 283 (2015) 416–422, <https://doi.org/10.1016/j.jpowsour.2015.02.131>.
- [17] H. Jiao, J. Wang, J. Tu, H. Lei, S. Jiao, Aluminum-ion asymmetric supercapacitor incorporating carbon nanotubes and an ionic liquid electrolyte: Al/AlCl₃-[EMIM]Cl/CNTs, *Energy Technol.* 4 (9) (2016) 1112–1118, <https://doi.org/10.1002/ente.201600125>.
- [18] N. Jayaprakash, S.K. Das, L.A. Archer, The rechargeable aluminum-ion battery, *Chem. Commun.* 47 (47) (2011) 12610–12612, <https://doi.org/10.1039/c1cc15779e>.
- [19] Z. Li, C. Gao, J. Zhang, A. Meng, H. Zhang, L. Yang, Mountain-like nanostructured 3D Ni₃S₂ on Ni foam for rechargeable aluminum battery and its theoretical analysis on charge/discharge mechanism, *J. Alloys Compd.* 798 (2019) 500–506, <https://doi.org/10.1016/j.jallcom.2019.05.270>.
- [20] X. Zhang, et al., Rechargeable ultrahigh-capacity tellurium-aluminum batteries, *Energy Environ. Sci.* 12 (6) (2019) 1918–1927, <https://doi.org/10.1039/c9ee00862d>.
- [21] S. He, D. Zhang, X. Zhang, S. Liu, W. Chu, H. Yu, Rechargeable Al-chalcogen batteries: status, challenges, and perspectives, *Adv. Energy Mater.* 11 (29) (2021) 1–14, <https://doi.org/10.1002/aem.202100769>.
- [22] X. Wen, et al., Materials compatibility in rechargeable aluminum batteries: chemical and electrochemical properties between vanadium pentoxide and chloroaluminate ionic liquids, *Chem. Mater.* 31 (18) (2019) 7238–7247, <https://doi.org/10.1021/acs.chemmater.9b01556>.
- [23] H. Jiao, D. Tian, S. Li, C. Fu, S. Jiao, A rechargeable Al-Te battery, *ACS Appl. Energy Mater.* 1 (9) (2018) 4924–4930, <https://doi.org/10.1021/acsaem.8b00905>.
- [24] H. Wang, et al., Binder-free V₂O₅ cathode for greener rechargeable aluminum battery, *ACS Appl. Mater. Interfaces* 7 (1) (2015) 80–84, <https://doi.org/10.1021/am508001h>.
- [25] S. Gu, H. Wang, C. Wu, Y. Bai, H. Li, F. Wu, Confirming reversible Al³⁺ storage mechanism through intercalation of Al³⁺ into V₂O₅ nanowires in a rechargeable aluminum battery, *Energy Storage Mater.* 6 (2017) 9–17, <https://doi.org/10.1016/j.ensm.2016.09.001>.
- [26] L.D. Reed, E. Menke, The roles of V₂O₅ and stainless steel in rechargeable Al-ion batteries, *J. Electrochem. Soc.* 160 (6) (2013) A915–A917, <https://doi.org/10.1149/2.114306jes>.
- [27] Y. Oh, G. Lee, Y. Tak, Stability of metallic current collectors in acidic ionic liquid for rechargeable aluminum-ion batteries, *ChemElectrochem* 5 (22) (2018) 3348–3352, <https://doi.org/10.1002/celec.201800892>.
- [28] S. Wang, et al., Aluminum chloride-graphite batteries with flexible current collectors prepared from earth-abundant elements, *Adv. Sci.* 5 (4) (2018) 1–6, <https://doi.org/10.1002/advs.201700712>.
- [29] Y. Zhang, S. Liu, Y. Ji, J. Ma, H. Yu, Emerging nonaqueous aluminum-ion batteries: challenges, status, and perspectives, *Adv. Mater.* 30 (38) (2018), <https://doi.org/10.1002/adma.201706310>.
- [30] M.R. Palacin, Roadmap on multivalent batteries, *JPhys Energy* 6 (2024) 031501, <https://doi.org/10.1088/2515-7655/ad34fc>.
- [31] L.L. Chen, et al., Nonmetal current collectors: the key component for high-energy-density aluminum batteries, *Adv. Mater.* 32 (42) (2020) 1–8, <https://doi.org/10.1002/adma.202001212>.
- [32] Z. Yu, J. Tu, C. Wang, S. Jiao, A rechargeable Al/graphite battery based on AlCl₃/1-butyl-3-methylimidazolium chloride ionic liquid electrolyte, *ChemistrySelect* 4 (11) (2019) 3018–3024, <https://doi.org/10.1002/slct.201900374>.
- [33] J. Liu, Z. Li, X. Huo, J. Li, Nanosphere-rod-like Co₃O₄ as high performance cathode material for aluminium ion batteries, *J. Power Sources* 422 (February) (2019) 49–56, <https://doi.org/10.1016/j.jpowsour.2019.03.029>.
- [34] J. Rodríguez-Carvajal, Recent advances in magnetic structure determination by neutron powder diffraction, *Phys. B Phys. Condens. Matter* 192 (1–2) (1993) 55–69, [https://doi.org/10.1016/0921-4526\(93\)90108-1](https://doi.org/10.1016/0921-4526(93)90108-1).
- [35] Y. Yasaka, C. Wakai, N. Matubayasi, M. Nakahara, Water as an in situ NMR indicator for impurity acids in ionic liquids, *Anal. Chem.* 81 (1) (2009) 400–407, <https://doi.org/10.1021/ac801767u>.
- [36] D.G. Farnum, Charge density-NMR chemical shift correlations in organic ions, *Adv. Phys. Org. Chem.* 11 (C) (1975) 123–175, [https://doi.org/10.1016/S0065-3160\(08\)60341-X](https://doi.org/10.1016/S0065-3160(08)60341-X).
- [37] S. Tan, et al., Complexation of heavy metal cations with imidazolium ionic liquids lowers their reduction energy: implications for electrochemical separations, *Green Chem.* 26 (3) (2023) 1566–1576, <https://doi.org/10.1039/d3gc03713d>.
- [38] B. Schwarz, Q. Fu, Magnetic single-ion anisotropy and Curie-Weiss behaviour of Mg₃V₄(PO₄)₆, *Eur. J. Inorg. Chem.* 27 (18) (2024), <https://doi.org/10.1002/ejic.202400162>.
- [39] Z. Misirlioğlu, A. Aksüt, Corrosion of molybdenum in aqueous media, *Corrosion* 58 (11) (2002) 899–903, <https://doi.org/10.5006/1.3280779>.
- [40] J. Fritscher, P. Hrobárik, M. Kaupp, Computational studies of electron paramagnetic resonance parameters for paramagnetic molybdenum complexes. 1. Method validation on small and medium-sized systems, *J. Phys. Chem. B* 111 (17) (2007) 4616–4629, <https://doi.org/10.1021/jp070638y>.
- [41] J. Estager, J.D. Holbrey, M. Swadzba-Kwasny, Halometallate ionic liquids-revisited, *Chem. Soc. Rev.* 43 (3) (2014) 847–886, <https://doi.org/10.1039/c3cs60310e>.
- [42] H. Lang, J. Zhang, Y. Kang, S. Chen, S. Zhang, Effects of lithium bis(oxalato)borate on electrochemical stability of [Emim][Al₂Cl₇] ionic liquid for aluminum electrolysis, *Ionics* 23 (4) (2017) 959–966, <https://doi.org/10.1007/s11581-016-1889-5>.
- [43] H. Hartmann, H.J. Schmidt, Über Absorptionsspektren komplexer Verbindungen des dreiwertigen Molybdäns, *Zeitschrift für Phys. Chemie* 11 (3–4) (1957) 234–250, <https://doi.org/10.1524/zpch.1957.11.3.4.234>.
- [44] T.B. Scheffler, C.L. Hussey, K.R. Seddon, C.M. Kear, P.D. Armitage, Molybdenum chloro complexes in room-temperature chloroaluminate ionic liquids: stabilization

- of [MoCl₆]²⁻ and [MoCl₆]³⁻, *Inorg. Chem.* 22 (15) (1983) 2099–2100, <https://doi.org/10.1021/ic00157a001>.
- [45] H. Sun, W. Wang, Z. Yu, Y. Yuan, S. Wang, S. Jiao, A new aluminium-ion battery with high voltage, high safety and low cost, *Chem. Commun.* 51 (59) (2015) 11892–11895, <https://doi.org/10.1039/c5cc00542f>.
- [46] J. Shi, J. Zhang, J. Guo, Avoiding pitfalls in rechargeable aluminum batteries research, *ACS Energy Lett.* 4 (9) (2019) 2124–2129, <https://doi.org/10.1021/acsenergylett.9b01285>.
- [47] A.M. Diem, B. Fenk, J. Bill, Z. Burghard, Binder-free v₂o₅ cathode for high energy density rechargeable aluminum-ion batteries, *Nanomaterials* 10 (2) (2020) 1–15, <https://doi.org/10.3390/nano10020247>.
- [48] X. Zhang, et al., Rechargeable ultrahigh-capacity tellurium-aluminum batteries, *Energy Environ. Sci.* 12 (6) (2019) 1918–1927, <https://doi.org/10.1039/c9ee00862d>.
- [49] J.G. Choi, L.T. Thompson, XPS study of as-prepared and reduced molybdenum oxides, *Appl. Surf. Sci.* 93 (2) (1996) 143–149, [https://doi.org/10.1016/0169-4332\(95\)00317-7](https://doi.org/10.1016/0169-4332(95)00317-7).
- [50] D.E. Couch, A. Brenner, Preparation of trichloride and tetrachloride of molybdenum, *J. Res. Natl. Bur. Stand. Sect. A Phys. Chem.* 63A (2) (1959) 185, <https://doi.org/10.6028/jres.063a.013>.